Received 26 April 2016; | Revised 6 June 2016; | Accepted 6 June 2016

DOI: xxx/xxxx

ARTICLE TYPE

Development of an improved parameter fitting method for planar biaxial testing using rakes

Heleen Fehervary* | Jos Vander Sloten | Nele Famaey

[1]Biomechanics Section, KU Leuven, Celestijnenlaan 300C, 3001 Heverlee, Belgium

Correspondence
*Heleen Fehervary Email: heleen.fehervary@kuleuven.be

Abstract

A correct estimation of the material parameters from a planar biaxial test is crucial since they will affect the outcome of the finite element model in which they are used. In a virtual planar biaxial experiment, a difference can be noticed in the stress calculated from the force measured experimentally at the rakes and the actual stress at the center of the sample. As a consequence, a classic parameter fitting does not result in a correct estimation of the material parameters. This difference is caused by the boundary conditions of the set-up and is among others dependent on the sample material. To overcome this problem, a new parameter fitting procedure is proposed that takes this difference into account by calculating a finite element-based correction vector.
This paper describes the methodology to apply this new parameter fitting procedure on real experimental data from a planar biaxial test using rakes. To this end, image processing is used to extract the experiment characteristics. This information is used to construct a finite element model. Two variations of the new parameter fitting procedure are investigated using two human aortic samples: a basic and an image-based approach. The performance of the method is assessed by the difference between the force measured at the rakes during the experiment and the force at the rakes obtained from the finite element simulation.
Both approaches of the new parameter fitting procedure lead to an improved estimation of the sample behavior compared to the classic approach.

KEYWORDS:
constitutive modeling, planar biaxial testing, rakes, parameter fitting, FE simulations, Boundary Conditions Corrected parameter fitting

1 | INTRODUCTION

Finite element (FE) modeling is an important tool within the field of biomedical engineering. It offers the possibility to accurately predict the patient-specific outcome of a medical device or treatment. Moreover, the use of *in silico* models in the development of a new device or treatment will allow a reduction in the number of clinical and animal trials. An important input for FE modeling is the material model, which requires mechanical characterization and constitutive modeling of soft biological tissues. However, the focus in this research domain lies mostly on characterizing different biological materials whereas research on the methodology itself is limited.
Regarding the methodology of planar biaxial testing most research is directed at investigating the difference between gripping

mechanisms (e.g. clamps, sutures or tethers and rakes) and sample shapes and the implications of the boundary conditions on the stress-strain field. Waldman and Michael Lee compared sutures and clamps experimentally and noted the big influence of the boundary conditions on the measured data[?]. Clamps and sutures were also compared using FE simulations by Sun *et al.*[?], who advised for the use of sutures because of the strong boundary conditions' effects when clamps are used. Attachment details in a planar biaxial test using rakes, such as varying number of rakes and inter-rake spacing, were studied by Eilaghi *et al.* and Fehervary *et al.* using a series of FE simulations[??]. A strong influence of attachment details on the uniformity of the strain field was observed[?]. Jacobs *et al.* noticed the difference between the stress measured at the clamps and the stress in the center of the sample using a FE simulation and proposed a correction factor to compensate for this difference[?]. In our previous study we noticed a similar difference in a FE simulation of a planar biaxial test using rakes: the stress calculated from the force measured experimentally at the rakes did not match the stress at the center of the sample. Since this difference depends on the material being tested, we proposed a new parameter fitting approach that estimates this difference using a FE model of the experiment[?]. This procedure is referred to as the Boundary Conditions Corrected (BCC) parameter fitting[a], since the difference in stresses is a consequence of the boundary conditions.

In general two categories of parameter fitting methods can be distinguished: using a forward or an inverse approach. In a forward approach, the objective function is a closed form function of the optimization variables and the optimization problem can be solved analytically. In the inverse approach, the objective function can no longer be solved analytically and often FE simulations are used to overcome this problem. The simplifications made in the data processing are the most important drawback of the forward or classic parameter fitting method. These simplifications do not have to be made in the inverse FE parameter fitting method, but this method has a high computational cost and often suffers from convergence issues. The BCC parameter fitting method combines the benefits of both approaches: using the forward method to solve the optimization problem efficiently and using a FE simulation to correct for the simplifications made in the data processing. As such, the BCC parameter fitting method can be located in between the two categories of parameter fitting methods.

The goal of this paper is to describe and evaluate the methodology to apply the BCC parameter fitting approach to a rake-based planar biaxial experiment. The materials and methods section first starts with an explanation of the procedure. Then the steps to go from a planar biaxial experiment towards the classic and the new parameter fitting procedure are explained. Next the results of each of these steps are shown and discussed. Finally, a conclusion is formulated.

2 | MATERIALS AND METHODS

This section starts by explaining the relevance of BCC parameter fitting. Then, all steps from a planar biaxial experiment up to BCC parameter fitting are explained. First, details are given on the two samples considered in this study and on the planar biaxial testing of these samples. Next, the steps for a classic parameter fitting are explained: the calculation of the strain during the test, the material model considered, and the objective function used in the classic parameter fitting approach. Afterwards, the extra developments for BCC parameter fitting are elaborated on: image processing of the sample to construct a FE model, the calculation of the correction vector and a stop-criterion for the convergence of the BCC parameter fitting approach. Finally, the BCC parameter fitting procedure and quality measures to assess the results are described.

2.1 | Relevance of BCC parameter fitting

In our previous study we investigated, among others, the best approach for data processing of a rake-based planar biaxial test using a virtual experiment[?]. The experiment was modeled using FE which allowed us to measure the stress at the center of the sample. In a real experiment, this stress cannot be measured, but the stress can be calculated from the force measured experimentally at the rakes. The stress at the center of the sample is referred to as the ground truth model stress and the one obtained from the rake forces is referred to as the experimental stress. Figure 1 shows that a difference between both stresses could be observed even in the virtual experiment with ideal dimensions.

This difference had serious implications on the parameter fitting. In a real experiment, only the experimental stress can be measured and a classic parameter fitting assumes that the stress at the center of the sample is the same as the experimental stress. More specifically, the material parameters are altered until the model stress at the center of the sample approximates the

[a]Previously referred to as Inhomogeneity from Experimental set-up Corrected (IEC) parameter fitting procedure in [?]

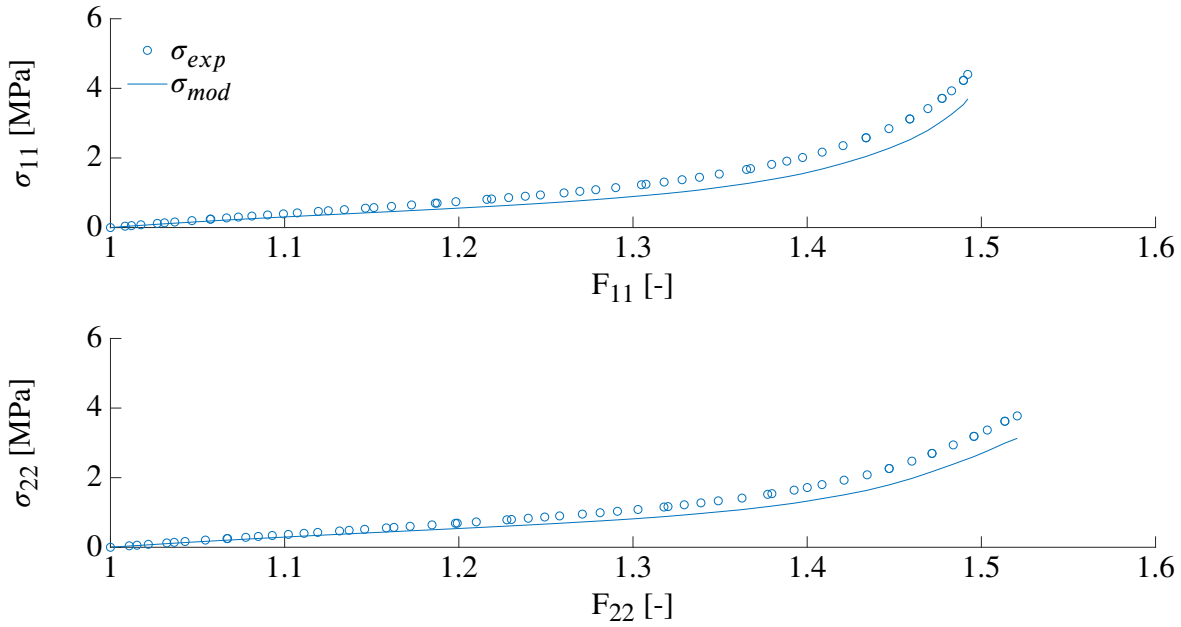

FIGURE 1 From a virtual planar biaxial experiment a difference can be observed between the experimental stress calculated from the force measured at the rakes and the ground truth model stress at the center of the sample.

TABLE 1 Parameter fitting result of a virtual planar biaxial test of a sample with the ground truth material parameters. The ground truth parameters cannot be found using a classic parameter fitting approach. Adapted from[?]

SET	C_{10} [MPa]	k_1 [MPa]	k_2 [-]	α[°]	κ [-]
Ground truth	0.0190	5.1500	8.6400	38.80	0.2400
Classic	0.0651	6.1790	9.3304	37.59	0.2573
BCC1	0.0124	5.1329	8.6350	38.87	0.2396

experimental stress as closely as possible. This implied that the ground truth material parameters could not be found with the classic parameter fitting (see Table 1).

The difference between the experimental and ground truth model stress depended, among others, on the positions of the rakes, the loading protocol and the sample material being tested. Therefore, it is impossible to define a single calibration factor that corrects for this difference. The BCC parameter fitting procedure estimates a correction vector for this difference based on a FE model of the experiment and takes this correction vector into account in the optimization of the material parameters. This is explained in detail in Section 2.9 and Figure 7 . This method has been applied to a virtual rake-based planar biaxial test and showed an improved approximation of the ground truth material parameters (see Table 1)[?]. The importance of the method was highlighted again when misalignment of the sample with respect to the test axes was investigated[?].

2.2 | Planar Biaxial Experiments

The two samples used in this study were tested previously within the framework of another study[?]. Healthy human aortic tissue was collected with the approval of the ethical committee of University Hospital Leuven (s51577). Patient details on the collected tissue are given in Table 2 .

After harvest, the tissue was stored at -80°C, immersed in Phosphate Buffered Saline (PBS). Before testing, the tissue was thawed overnight at 4°C. From the harvested tissue, the circumferential and longitudinal direction could be retrieved. Square samples with a sample length L_s of at least 7 mm were dissected with the sample orientation such that the test axes of planar biaxial set-up were aligned with the circumferential and longitudinal direction. The thickness of the sample H was measured

TABLE 2 Details on the collected tissues

SAMPLE	sex	age [years]	weight [kg]	height [cm]	BMI [kg/m^2]
S1	M	21	70	180	21.60
S2	M	48	75	180	23.15

using image analysis on a picture of the sample placed in between two metal plates with known thickness (see Figure 2 and Table 4). Next, five markers were attached to the central area of the sample using surgical wire and glue.

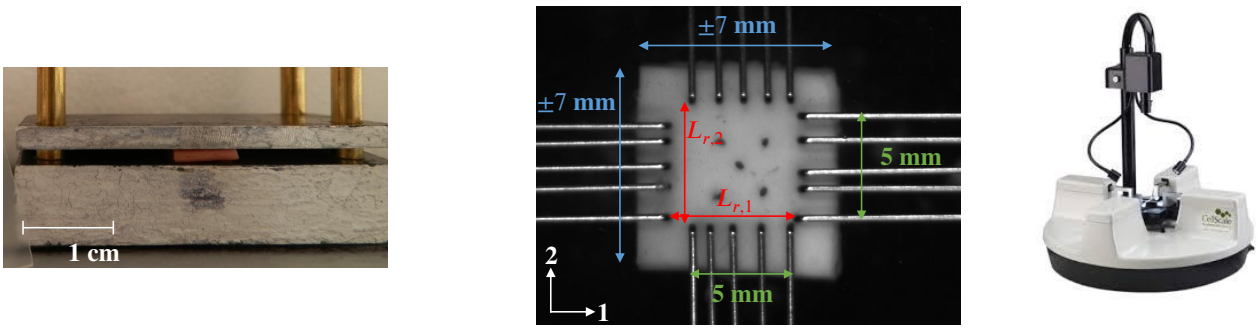

FIGURE 2 Details on the planar biaxial testing. Left: to measure the sample thickness the sample is placed between two plates; the thickness of the top plate is known and the sample thickness can be determined using image processing. Middle: sample mounted in the set-up using rakes. Markers in the center of the sample are used for strain measurement. Right: the planar biaxial testing device used: BioTester 5000, CellScale.

The samples were tested in a planar biaxial set-up (BioTester 5000, CellScale, Waterloo, Canada). The set-up was equipped with four linear actuators and two load cells (one per test axis). The range of the load cell was 23 N with an accuracy of 0.2% of the full range (i.e. 46 mN). The sample rate of the actuators and load cells was 30 Hz. A camera (1280 by 960 pixels) continuously took pictures during the test at a frame rate of 15 Hz. The sample was mounted using four BioRakes (CellScale) with each five rakes, spaced 1 mm apart and a rake diameter of 0.3 mm. During the test, the sample was immersed in 0.9% NaCl solution at room temperature. In the force controlled protocol an increasing force was applied with different ratios (see Table 3). Multiple cycles were applied to account for the softening effect of soft biological tissues. At the beginning of each set, a preload of 70 mN was applied to avoid sagging of the sample.

The output data from the experiment were: force measurements at the rakes, displacements of the rakes and the images made with the camera.

The selected data that was used for post processing, is shown in Table 4 . The length covered by the rakes in the i-th direction $L_{r,i}$ (see Figure 2) and the loaded surface with the normal in the j-direction A_j for the corresponding sample and set are also shown. A_j was calculated from the sample thickness H and $L_{r,i}$. Note that these measurements were defined in the initial or reference state (i.e. after the preload has been reached).

2.3 | Strain calculation: deformation gradient

The deformation of the sample was assumed to be planar, hence only one camera perpendicular to the tissue was used. The strain can be calculated using displacements of markers or rakes. When the strain is measured based on the markers, tear that occurs at the rake holes is accounted for, while this is not the case when the rakes are used.

TABLE 3 Protocol of the planar biaxial test: force applied in the 11- and 22-direction (i.e. the circumferential and axial direction, respectively), duration of the slope over which this force is applied and number of times these conditions were repeated.

SET	11-Force [N]	22-Force [N]	duration [s]	# cycles
F1-1	0.7	0.7	1	10
F2-2	1.4	0.7	2	5
F2-1	1.4	1.4	2	5
F2-0.5	1.4	1.4	2	5
F4-2	2.8	1.4	4	5
F4-1	2.8	2.8	4	5
F4-0.5	1.4	2.8	4	5
F8-2	5.6	2.8	8	5
F8-1	5.6	5.6	8	5
F8-0.5	2.8	5.6	8	5

TABLE 4 Selected set, sample thickness, and corresponding length covered by the rakes in the i-th direction L_{ri} and loaded surface A_j with the normal in the j-th direction.

SAMPLE	selected set	thickness H [mm]	$L_{r,1}$ [mm]	$L_{r,2}$ [mm]	A_1 [mm^2]	A_2 [mm^2]
S1	F4-1	2.13	5.76	5.31	11.32	12.28
S2	F4-1	2.44	5.86	5.44	13.27	14.29

2.3.1 | Markers

The strain at the center of the sample was measured using the method of Hoffman[?]. In this method the four outer markers build up a two dimensional element. Using marker displacements and shape functions, the strains in the deformed element could be calculated. These correspond to the components in the 1- and 2-directions.

Assuming incompressibility, the strain through the thickness was calculated. In this case, there was no volume change and $\det(\boldsymbol{F}) = J = 1$. Hence, the strain for the 33-component was

$$F_{33} = \frac{1}{F_{11}F_{22} - F_{12}F_{21}}. \tag{1}$$

The other components related to the 3-direction were assumed to be zero. The deformation gradient based on the markers $\boldsymbol{F}_m$ was then

$$\boldsymbol{F}_m = \begin{bmatrix} F_{11} & F_{12} & 0 \\ F_{21} & F_{22} & 0 \\ 0 & 0 & F_{33} \end{bmatrix} \tag{2}$$

The marker displacements in the 1- and 2-direction were tracked from the images using an in-house developed software in Matlab 2017a (The Mathworks Inc., Natick, Massachusetts, USA).

2.3.2 | Rakes

The ij-th component of the deformation gradient was calculated as follows:

$$F_{ij} = \delta_{ij} + u_{i,j}. \tag{3}$$

with δ_i the Kronecker delta and $u_{i,j}$ the displacement in the i-th direction of the surface with the normal in the j-th direction. The rakes were only displaced in the normal direction. Hence, the deformation gradient based on the rakes $\boldsymbol{F}_r$ was then:

$$\boldsymbol{F}_r = \begin{bmatrix} 1 + u_{1,1} & 0 & 0 \\ 0 & 1 + u_{2,2} & 0 \\ 0 & 0 & F_{33} \end{bmatrix} \tag{4}$$

Where F_{33} was again calculated using the incompressibility assumption:

$$F_{33} = \frac{1}{(1+u_{1,1})(1+u_{2,2})}. \tag{5}$$

2.4 | Material model

The Gasser-Ogden-Holzapfel (GOH) material model[?], designed to model arterial tissue, was chosen to model the mechanical behavior of the aortic tissue. The GOH material model defines a strain energy density function Ψ that is composed out of a linear isotropic part and a non-linear anisotropic part,

$$\Psi = C_{10}(I_1 - 3) + \sum_{i=4,6} \frac{k_1}{2k_2}\left[e^{k_2(\kappa I_1 + (1-3\kappa)I_i - 1)^2} - 1\right]. \tag{6}$$

The isotropic part represents the elastin matrix and corresponds to the Neo-Hookean material model. I_1 is the first invariant of the right Cauchy-Green deformation tensor $\boldsymbol{C} = \boldsymbol{F}^T\boldsymbol{F}$. C_{10} is a material parameter corresponding to the stiffness of the matrix. The anisotropic part consists out of two collagen fibers families. I_4 and I_6 are pseudo-invariants corresponding to the stretch in the direction of the fiber and calculated as: $I_i = \boldsymbol{C}(M_i \cdot \boldsymbol{C})$. M_i is the fiber vector of the i-th fiber family, defined using a fiber angle α_i with respect to the circumferential direction,

$$M_i = \begin{bmatrix} \cos\alpha_i \\ \sin\alpha_i \\ 0 \end{bmatrix}. \tag{7}$$

The fiber families were assumed to be symmetric with respect to the circumferential direction: $\alpha_4 = -\alpha_6$. k_1 is a material parameter corresponding to the stiffness of the fibers. k_2 is a material parameter related to the non-linearity. κ is a parameter related to the dispersion of the fibers. C_{10}, k_1 and k_2 have a positive value. κ has a value between 0 (i.e. no dispersion), and $1/3$ (i.e. fully dispersed fibers and thus isotropic behavior).

The first Piola-Kirchhoff stress $\boldsymbol{P}$ was calculated from Ψ as[?]

$$\boldsymbol{P} = -p\boldsymbol{F}^{-T} + \frac{\partial\Psi}{\partial\boldsymbol{F}}. \tag{8}$$

The hydrostatic pressure p is introduced for incompressible materials and is an indeterminate Lagrangian multiplier. p was determined from boundary conditions: for a planar biaxial test, a plane stress state was assumed, and hence $\sigma_{33} = 0$. The Cauchy stress $\boldsymbol{\sigma}$ was calculated from $\boldsymbol{P}$ as:

$$\boldsymbol{\sigma} = J^{-1}\boldsymbol{P}\boldsymbol{F}^T, \tag{9}$$

where $\boldsymbol{J}$ was the the Jacobian or volume-change, as mentioned before.

Finally, the model traction force $\boldsymbol{t}$ was calculated from the first Piola-Kirchhoff stress[?] as

$$t_{ij} = P_{ij}A_j, \tag{10}$$

with t_{ij} the force in the i-th direction, applied on a surface with the normal in the j-th direction. A_j was the loaded surface with the normal in the j-th direction in the reference state (see Table 4). Note that no Einstein notation was used in Equation 10, hence there was no summation over j. Moreover, other engineering disciplines might use a different convention.

2.5 | Classic parameter fitting

In classic parameter fitting the material parameters of the model were altered until the model matched the experimental data as closely as possible. In this case traction forces $\boldsymbol{t}$ were optimized and the objective function O of this optimization problem was

$$O = \sum_{c=11,22} (w_c(t_c^{mod} - t_c^{exp}))^2, \tag{11}$$

with c the objective components: 11 and 22 for a planar biaxial test. The weights w_c were calculated for each objective component and compensated for a difference in force range between different components. It was calculated as the lowest of the maximum traction forces of all objective components over the maximum force of that objective component. Since in this case

TABLE 5 The boundaries for the material parameters of the GOH model.

BOUNDARIES	C_{10} [MPa]	k_1 [MPa]	k_2 [-]	κ [-]	α [RAD]
lower	1e-4	0	1e-4	0	0
upper	1	10	100	1/3	π

an equibiaxial loading set of a force-controlled protocol was considered, the maximum forces were similar in the 11- and 22-direction and the weights were close to 1.

Table 5 shows the boundaries of the material parameters of the GOH model that were optimized. The lower boundaries of C_{10} and k_2 were chosen to be different from 0 as the FE software Abaqus (Dassault Systèmes Simulia Corp., Providence Rhode Island, USA) did not accept these parameters to be 0. The upper boundaries of the parameters were not based on a physical limit, but were far above the values that are typically found.

The parameter fitting code was implemented in Matlab and the optimization problem was solved with the CasAdi toolbox[?] using Optistack[?]. To assure that a global minimum was found, 10 different initial starting points were used.

2.6 | Image processing

From the images of the experiment, the sample contour, the insertion points of the rakes (further referred to as rake holes), the orientation of the rakes and the markers needed to be detected to create a FE model of the experiment. All image processing was conducted in Matlab using available Matlab functions. Since the contrast in the image was good (see Figure 2), simple image processing techniques such as thresholding, erosion and dilation of objects were sufficient. Note that an erosion was always followed by an equal dilation of the image, such that the dimensions of the object were re-established. The image processing was applied on the reference image (i.e. the first image of the set).

2.6.1 | Sample contour

The steps to detect the sample contour are shown in Figure 3 . First an erosion was applied on the image, such that the rakes were blurred. A global threshold was then applied, allowing to segment the sample. A combination of dilations and erosions was then used to fill up the sample areas that were covered by the rakes. From this a first sample contour could be extracted. Next, an adaptive threshold was applied on the region surrounding the first sample contour. This led to a second sample contour with an increased the accuracy. However, sometimes parts of rakes were also segmented in this second detection. Therefore, both segmentations were presented to the user, who could decide on the best segmentation for this particular sample.

FIGURE 3 Steps in the image processing to detect the sample contour from the image.

2.6.2 | Rake holes

Figure 4 shows the method to detect the rake hole. First the rakes were detected by extracting a region of interest in which only the rakes at one side without the sample were visible. A global threshold could then be applied on this region of interest and the five rakes could be detected. Each rake was then approximated by a line, based on the detected part of the rakes. This line was

extrapolated to the sample region and a first guess of the rake hole location was found by selecting the last dark point one this line. An adaptive threshold was applied around this location. Image erosion and dilation were used to smooth the border of the detected area and its centroid was used as the coordinates of the rake hole.

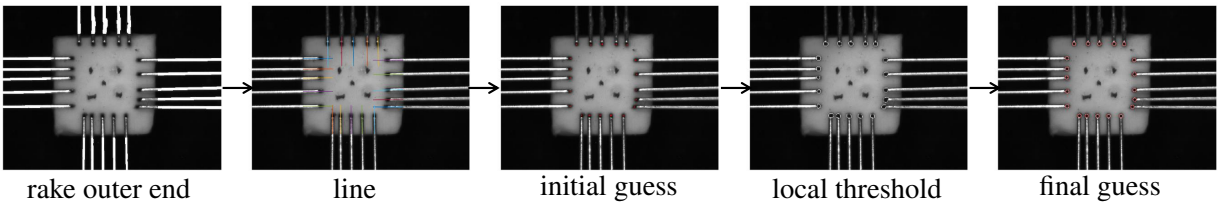

FIGURE 4 Methodology to detect the rake holes from the image

2.6.3 | Rake orientation

Due to wear and mounting, the spacing of the rakes at the tip, might not be completely uniform. However, at the base the spacing of the rakes is uniformly. Consequently, the rakes might have a small rotation with respect to the rakes' base. Hence, the orientation of each rake needed to be determined. Unfortunately, the rakes were not fully visible in the experimental images and some assumptions needed to be made. As shown in Figure 5 , the base point of the middle rake was estimated as 30 mm in the normal direction from the averaged rake hole (i.e. the average of the rake holes at one side). From this point, the other base points were spaced 1 mm apart. The orientation of each rake was determined from the point at the rakes' base and the position of the rake hole.

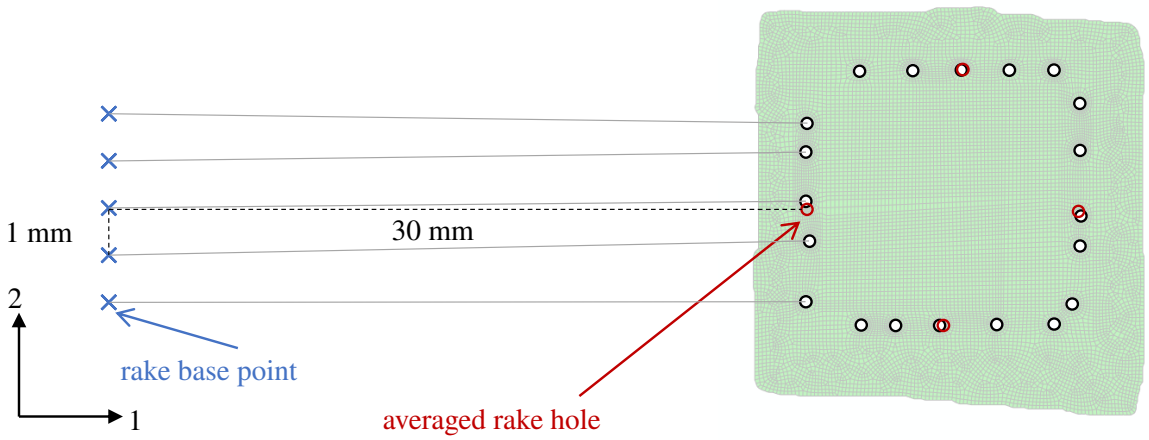

FIGURE 5 The rake orientations were determined based on the rake hole and the rake base point.

2.6.4 | Markers

The markers could be detected by defining a region of interest in the central area of the sample. A global threshold then allowed to segment the five markers. Again image erosion and dilation were used to smooth the border of the marker. The centroid was used as the coordinates of the marker.

2.6.5 | Scaling factor: from pixel to mm

The cameras were not calibrated at the start of the test. Hence, it was necessary to scale the coordinates of the sample contour, the rake holes and the markers from pixels to mm. In between different tests, the position of the cameras was not changed. The only known dimension in the images was the width of the rakes: here 0.3 mm. As the visibility of the contours of the rakes depended on the lighting conditions, the maximum width of the rakes was tracked in several images and from this a scaling factor was calculated to convert the coordinates of sample contour, rake holes and markers to mm.

2.7 | Finite element model

Two FE models were constructed in Abaqus 6.14: a basic and a image-based planar biaxial experiment using rakes. Both FE models were constructed in the same way, only the input data is different. The input data for the image-based model was based on the image processing: the sample contour, the rake holes and orientations and the markers. For the basic FE model this data was approximated with the data available from the experiment. The sample contour was approximated as a square with length L_s (in this case 7 mm as mentioned before). The coordinates of the rake holes were obtained from the length covered by the rakes L_r; this is an output of the experiment, based on the position of the actuators. The rake holes were placed evenly spaced in the sample contour. The markers were placed symmetrically at the 20% central area of the sample: four making up a square and one at the center.

An automated Python script was developed to construct both FE models. The sample was created based on the sample contour. Rake holes were constructed as circles with a diameter of 0.3 mm (i.e. the diameter of a rake). The markers were defined as the nodes closest to the markers' coordinates. The sample was modeled as a 3D deformable shell with membrane elements (M3D4). Membrane elements are surface elements that transmit in-plane forces and have no bending stiffness[?].

A mesh convergence analysis was performed as follows: the total number of elements was increased by increasing the number of elements on the sample contour. The sample was then uniformly meshed with the average seedsize of the elements on the contour. Convergence was reached when the convergence error between the mean correction vector of the previous mesh and the current mesh was below 1%. The mean correction vector was defined as the ratio between the traction force measured experimentally at the rakes and the model traction force calculated as described in Section 2.4 from the deformation gradient $\boldsymbol{F}_m$ and the material parameters. Mesh convergence was reached for 4962 and 5678 elements for the basic FE model and for 21 321 and 7594 elements for the image-based FE model of sample S1 and S2, respectively. The sample material was modeled using the GOH material model that is implemented in Abaqus.

The rakes were modeled as a 3D deformable wire with a circular cross section with a radius of 0.15 mm. The length of the rake was 30 mm and B33 elements were used. These elements can be used to model slender beams, where the cross-section is small compared to the axial length[?]. In a second mesh convergence study the number of elements of these rakes were doubled. Using the same criterion as before, mesh convergence of the rakes was reached at 63 elements. The rake material was Tungsten and was modeled as linear elastic with a Young's modulus of 400 GPa and a Poisson ratio of 0.28.

The rakes were connected to the sample using a kinematic coupling between the rake tip and a semi circle of the rake hole for the normal direction and between one point of the semi circle and the rake tipe for the normal and transverse direction (see Figure 6).

The rakes were displaced using a tabular amplitude in the boundary conditions. This amplitude was important as the biaxial loading conditions interfere with one another. The displacements of the actuators through time were available in the outputs of the experiment. These displacements were applied at the rake base points. The rakes were only displaced in the normal direction and the other degrees of freedom were fixed.

The simulation was conducted in Abaqus Standard with a time step such that at least 40 data points were available. The output of the simulation was the data that is available in a real planar biaxial experiment: the coordinates of the markers, the reaction forces at the rakes and the displacements of the rakes.

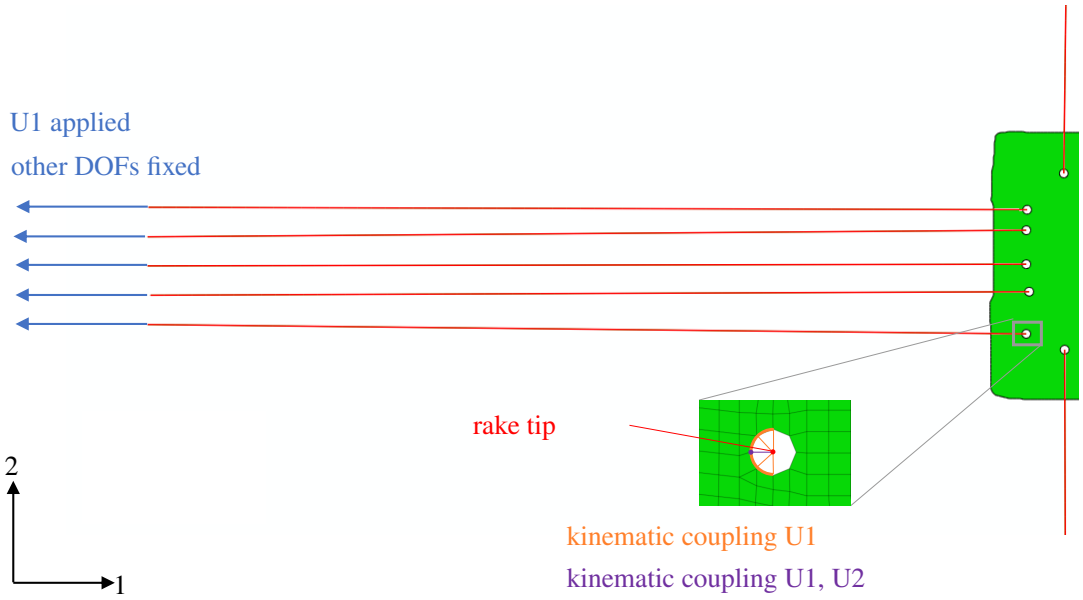

FIGURE 6 Boundary conditions of the FE model. The rake base points are displaced in the normal direction and the other DOFs are zero.

2.8 | Correction vector

As explained in Section 2.1, the FE simulation of a planar biaxial experiment revealed a difference between the stress calculated from the force measured experimentally at the rakes and the stress at the center of the sample. Since this difference depended, among others, on the sample material being tested, no single calibration factor could be defined that was generally applicable. To overcome this problem, a correction vector g_c for an objective component c could be calculated based on the outputs of a FE simulation of the experiment as

$$g_c = \frac{t^{FE}_{mod,c}}{t^{FE}_{exp,c}}. \tag{12}$$

g_c was a function of the strain and was applied to the planar biaxial test data. If necessary, the correction vector was resampled in function of the boundary conditions (i.e. the displacements of the rakes).

2.9 | BCC parameter fitting

Figure 7 shows a schematic overview of the BCC parameter fitting procedure. After a classic parameter fitting, a FE simulation of the planar biaxial test with the material parameters resulting from the classic fitting was conducted. The correction vector g_c was calculated from this FE simulation and was then applied to the experimental data. The objective function was then

$$O = \sum_{c=11,22} (w_c(t^{mod}_c - g_c \cdot t^{exp}_c))^2, \tag{13}$$

with c and w_c as before. Also the boundaries of the parameters and the optimization method was the same as before. Note that, as the material that was being tested was unknown, the correction vector was an approximation of the real correction vector. This iterative loop of conducting a FE simulation, calculating the correction vector and performing a new parameter fitting, was

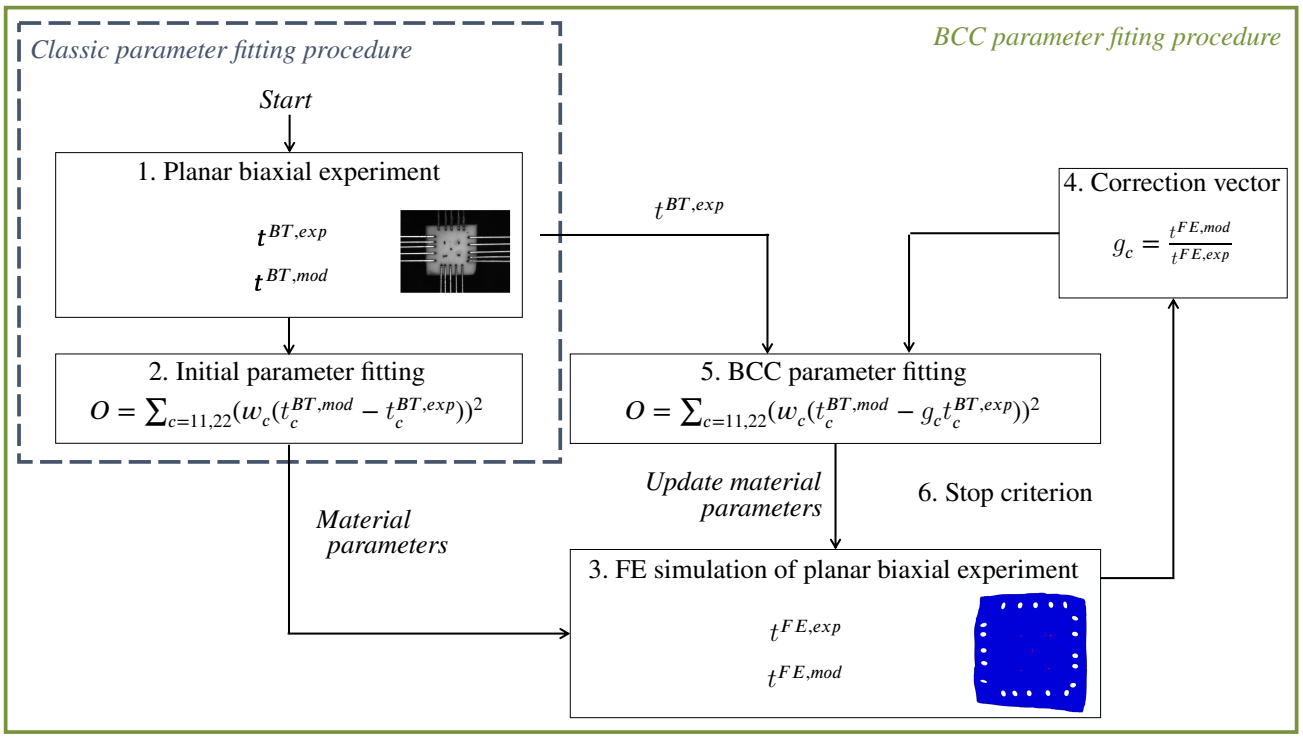

FIGURE 7 Schematic overview of the BCC parameter fitting procedure: after a classic parameter fitting, a FE simulation of the experiment is conducted with the material parameters resulting from the classic fitting. A correction vector is calculated from the FE simulation, which can then be applied on the planar biaxial testing data. This iterative loop is repeated until convergence is reached. Adapted from[?].

repeated until convergence was reached. The convergence of the correction vector was used as a stop criterion of this iterative loop. To this end, the root mean square error between the value of the correction vector of previous and the current iteration RMSE_g was calculated as

$$\text{RMSE}_g = \sqrt{\frac{1}{||c||}\sum_{c=11,22}(g_c^{t-1} - g_c^t)^2}, \tag{14}$$

with c the objective components (11 and 22 for a rake-based planar biaxial test) and t the current iteration. Convergence was reached when the RMSE_g is smaller than a certain threshold (in this case 0.001).

2.10 | Quality measures

Two measures were used to quantitatively evaluate the BCC parameter fitting procedure. First, the Mean Percentage Error (MPE) could be calculated between the material parameters obtained with the classic parameter fitting and those obtained with BCC parameter fitting (MPE_C) and was calculated as

$$\text{MPE}_C = \frac{1}{p}\sum_{i=1}^{p}\frac{P_{C,i} - P_{BCC,i}}{P_{C,i}}, \tag{15}$$

with p the number of material parameters (i.e. 5 for the GOH material model) and P_C and P_{BCC} the classic and BCC fitted parameters, respectively.

A second quality measure quantifies the difference between the experimental traction force measured in the planar biaxial experiment and the one from the FE simulation. The RMSE between both experimental forces was calculated as

$$\text{RMSE}_{t,exp} = \frac{1}{||c||} \sum_{c=11,22} \sqrt{\frac{1}{m} \sum_{i=1}^{m} (t^{BT}_{exp,c,i} - t^{FE}_{exp,c,i})}, \tag{16}$$

with c the objective components (i.e. 11 and 22 for a rake-based planar biaxial test) and m the number of entries in the vector t_{exp}.

3 | RESULTS

This section shows the results and starts with the classic parameter fitting. Then the results of the intermediate steps necessary for BCC parameter fitting are shown: the image processing, the FE models and the correction vector. Finally, the results of the BCC parameter fitting is shown in which two cases are considered: 1) basic BCC (BCC_b): using the basic FE model, and 2) image-based BCC (BCC_i): using an image-based FE model.

3.1 | Classic parameter fitting

Table 6 shows the material parameters of the GOH material model resulting from the classic parameter fitting procedure. The RMSE_O was the value of the objective for these material parameters and is thus a value for goodness of fit. This result is also shown in Figure 8 for both samples. The experimental Cauchy stress was calculated from the force measured experimentally at the rakes during the test and the model Cauchy stress was calculated from the fitted material parameters.

TABLE 6 Material parameters of the GOH model obtained with the classic parameter fitting procedure.

SET	C_{10} [MPa]	k_1 [MPa]	k_2 [-]	κ [-]	α [RAD]	RMSE_O [-]
S1	0.0224	0.0081	1.2474	0.0000	0.6993	0.3859
S2	0.0166	0.0614	32.2953	0.2568	0.0012	0.2774

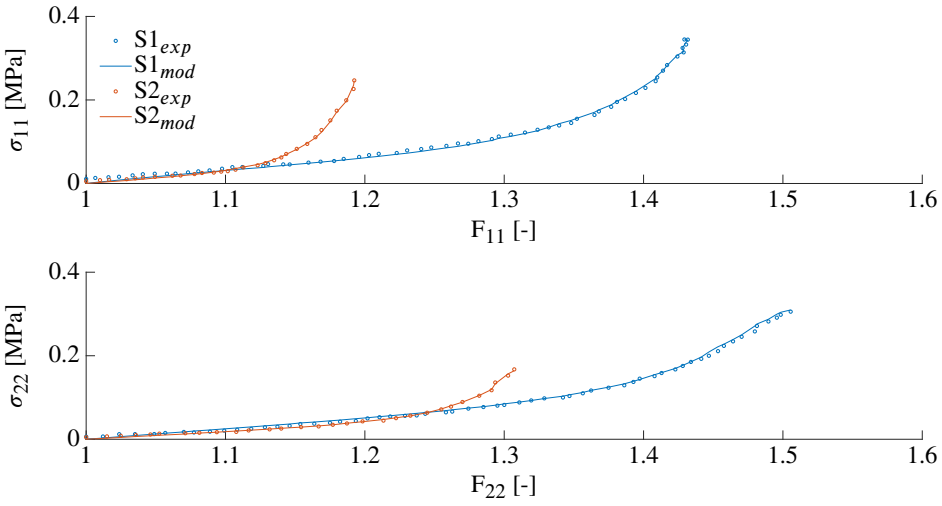

FIGURE 8 Result of the classic parameter fitting: the experimental and fitted Cauchy stresses for both samples. A good fit is obtained in both cases.

3.2 | Image processing

An automated procedure for image processing was developed to detect the sample contour, the rake holes and the markers. Figure 9 shows the images and the result of the image processing of both samples S1 and S2. A visual inspection showed that the elements were detected properly.

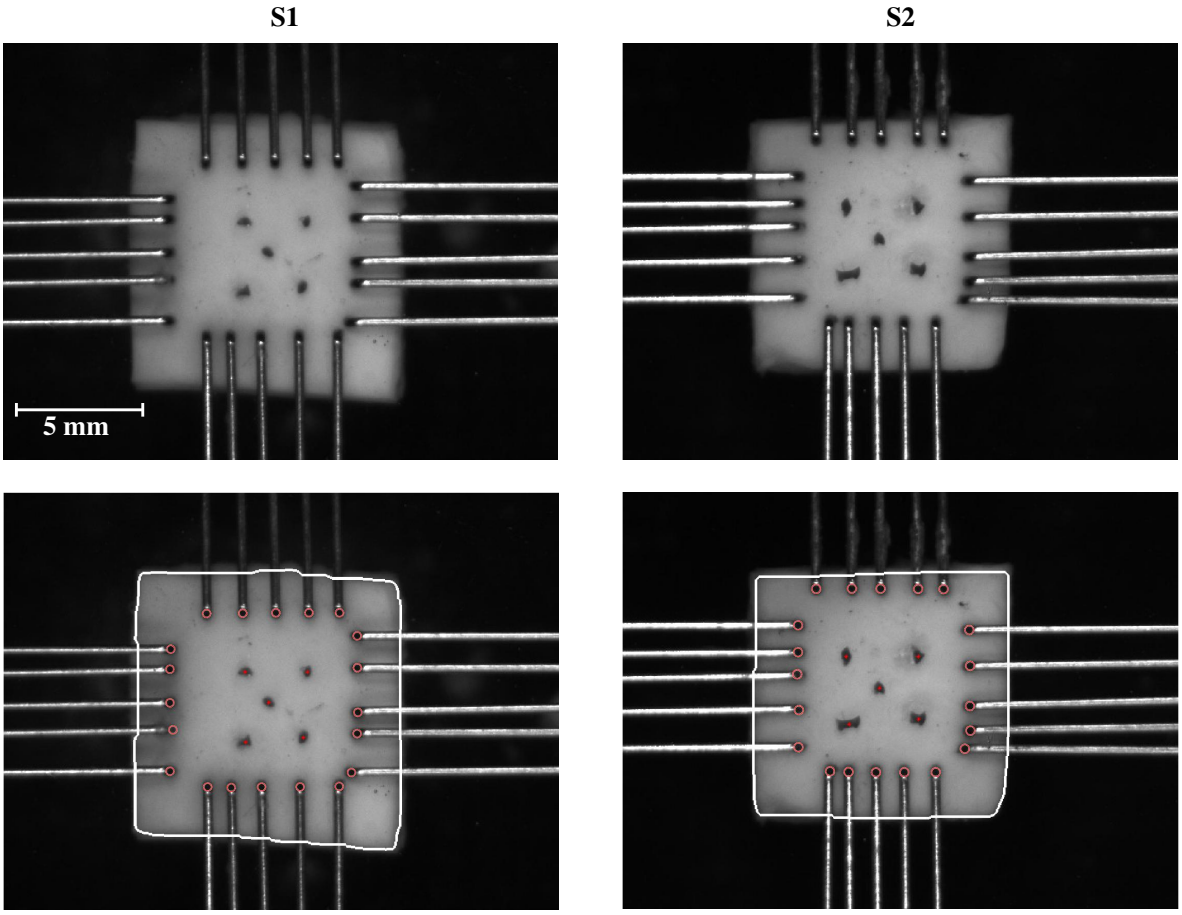

FIGURE 9 Result of the image processing of S1 and S2. The original image is shown at the top. The bottom shows an overlay with the results from image processing. The sample contour, the rake holes and the markers are detected with an automated procedure.

3.3 | Finite element models

Two types of FE models were constructed: a basic and an image-based FE model. Figure 10 shows a manual overlay of the deformed FE simulation and the deformed experimental picture of both samples. Both the basic and the image-based FE models are shown. It can be observed that the image-based version was a better approximation of the deformed state of the sample than the basic, especially concerning the location of the rake holes and the markers.

3.4 | BCC Parameter Fitting

Two variations of the BCC parameter fitting were investigated: 1) basic BCC (BCC_b): using a basic FE model, and 2) image-based BCC (BCC_i): using an image-based FE model. Tables 7 and 8 show the resulting material parameters obtained with

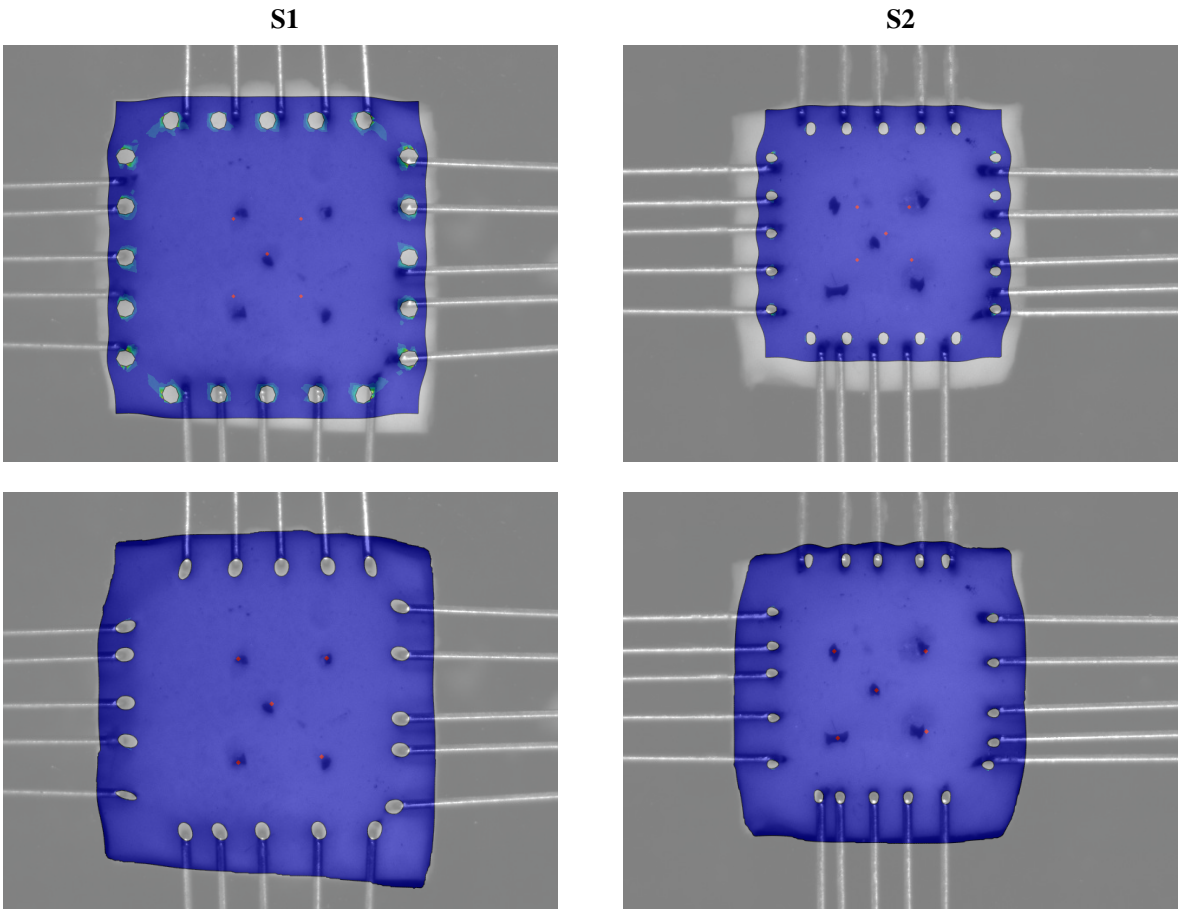

FIGURE 10 Overlay of the deformed state of the FE model with the experiment of samples S1 and S2. The basic FE models (top) show less correspondence with the experiment than the image-based FE models (bottom).

these two different cases. The low values of RMSE_O indicated that a good fit was obtained for every iteration, for both cases. The RMSE_g is also shown and allowed to observe the convergence of the BCC parameter fitting: with increasing BCC iterations, the values of RMSE_g decreased and thus the method converged. MPE_C quantified the difference between the fitted material parameters of a BCC iteration and the material parameters obtained with the classic parameter fitting. Finally, also $\text{RMSE}_{t,exp}$ is shown, which quantified the difference between the experimental traction force from the biaxial test and from the FE simulation. One could assume that the best approximation of the material was when the $\text{RMSE}_{t,exp}$ was the smallest. This was not always the last iteration of the BCC parameter fitting procedure. Both cases ended up in a different material parameter set. The traction force curves obtained with the final material parameters are shown in Figures 11 and 12 .

TABLE 7 Material parameters for the GOH model obtained with different approaches of the BCC parameter fitting procedure for sample S1.

Method	Fitting	C_{10} [MPa]	k_1 [MPa]	k_2 [-]	κ [-]	α [rad]	$RMSE_O$ [N]	$RMSE_g$ [-]	MPE_C [%]	$RMSE_{t,exp}$ [N]
BCC_b	C	0.0224	0.0081	1.2474	0.0000	0.6993	0.3859	-	-	0.3443
	BCC1	0.0208	0.0054	1.4522	0.0000	0.7059	0.3203	0.1187	11.57	0.2352
	BCC2	0.0209	0.0051	1.4913	0.0000	0.7054	0.3200	0.0036	12.83	0.2401
	BCC3	0.0209	0.0051	1.4980	0.0000	0.7053	0.3201	0.0005	12.94	-
BCC_i	C	0.0224	0.0081	1.2474	0.0000	0.6993	0.3859	-	-	0.2240
	BCC1	0.0193	0.0046	1.5253	0.0001	0.7085	0.3034	0.1841	16.13	0.0923
	BCC2	0.0196	0.0042	1.6083	0.0001	0.7078	0.3047	0.0066	18.16	0.1026
	BCC3	0.0196	0.0041	1.6285	0.0001	0.7076	0.3051	0.0020	18.73	0.1059
	BCC4	0.0196	0.0041	1.6331	0.0000	0.7076	0.3052	0.0005	18.80	-

TABLE 8 Material parameters for the GOH model obtained with different approaches of the BCC parameter fitting procedure for sample S2.

Method	Fitting	C_{10} [MPa]	k_1 [MPa]	k_2 [-]	κ [-]	α [rad]	$RMSE_O$ [N]	$RMSE_g$ [-]	MPE_C [%]	$RMSE_{t,exp}$ [N]
BCC_b	C	0.0166	0.0614	32.2953	0.2568	0.0012	0.2774	-	-	0.2399
	BCC1	0.0156	0.0574	33.7289	0.2600	0.0012	0.2681	0.0647	3.64	0.1996
	BCC2	0.0156	0.0572	33.8436	0.2601	0.0012	0.2682	0.0013	3.79	0.2005
	BCC3	0.0156	0.0572	33.8482	0.2601	0.0012	0.2682	0.0001	3.79	-
BCC_i	C	0.0166	0.0614	32.2953	0.2568	0.0012	0.2774	-	-	0.2008
	BCC1	0.0155	0.0645	38.2342	0.2743	0.0012	0.2785	0.0779	7.38	0.1493
	BCC2	0.0156	0.0625	39.1119	0.2748	0.0011	0.2771	0.0061	8.85	0.1502
	BCC3	0.0156	0.0621	39.2443	0.2748	0.0011	0.2774	0.0009	8.80	-

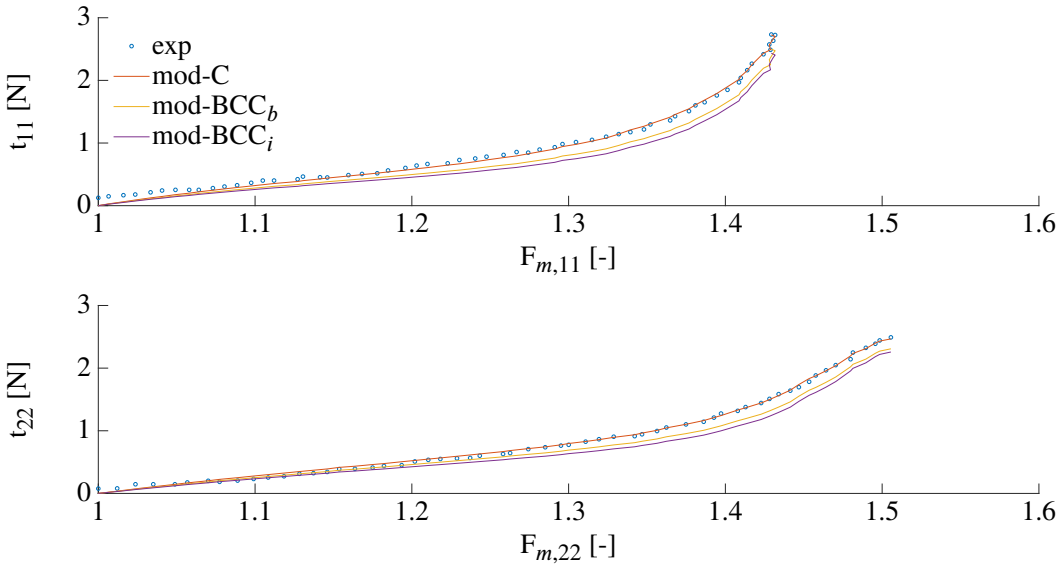

FIGURE 11 Experimental (exp) and model traction forces for sample S1 obtained with different fitting approaches: the classic procedure (mod-C) and two cases of the BCC procedure (mod-BCC_b and mod-BCC_i).

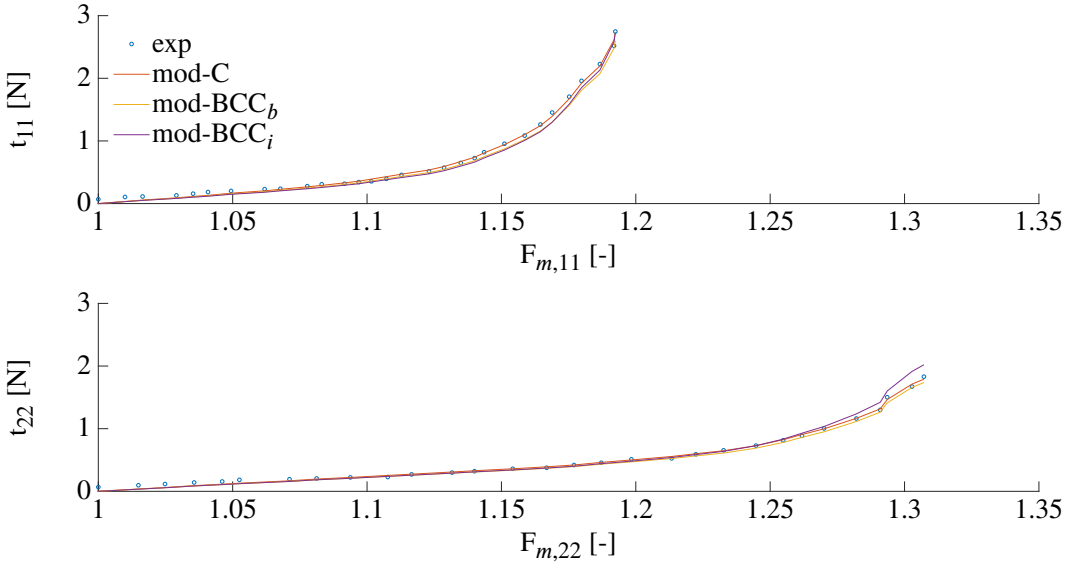

FIGURE 12 Experimental (exp) and model traction forces for sample S2 obtained with different fitting approaches: the classic procedure (mod-C) and two cases of the BCC procedure (mod-BCC$_b$ and mod-BCC$_i$).

4 | DISCUSSION

The BCC parameter fitting procedure was already applied on a virtual experiment of a rake-based planar biaxial test and shown to be effective in Fehervary *et al.*[?] . The aim of this study was to develop the BCC parameter fitting procedure for a real rake-based planar biaxial experiment. This section discusses the different methods that were applied and their results. First the image processing and FE simulation are discussed. Next the results of the Classic and BCC parameter fitting are compared and finally, some general elements are discussed. The actual material parameters of the two samples are not the main interest of this paper and are therefore not discussed further.

4.1 | Image processing and FE simulation

The goal of the image processing is to extract the sample contour, the rake holes and orientations, and the markers from an experimental image. The good contrast in the image helps in extracting these elements and a visual inspection of the results is used to assess whether the performance of the image processing is sufficient. However, some points of discussion and future improvements can be raised.

The sample contour is sometimes not consistent through the thickness (for example the top of sample S1 in Figure 9). This cannot be captured with one camera and hence we have assumed here that the sample contour is the one of the top surface. To be able to capture variation in the 3-direction, stereo vision is necessary. This would also allow to measure the out of plane deformation and to create a 3D FE model of the experiment.

The exact position of the rake holes can be subject to interpretation. Here, the dark area just behind the bended tip of the rake, is considered as the puncture point.

Only a part of the rakes is visible in the images and therefore some assumptions had to be made to determine the rake base points and the orientations of the rakes. In the future it would be better to have an image including a bigger part of the rakes.

Currently, the conversion from pixel to mm was based on the diameter of the rakes. However, the detected diameter of the rakes was very dependent on the lighting conditions. It would be better to add a calibration mark on the set-up (e.g. on the rakes).

Since the current code is dependent on the contrast in the image, strong variations in the lighting conditions or the contrast will affect its performance. Some adaptations might be required for it to be used for similar set-ups with different lighting conditions. Clearly, a minimum amount of contrast will always be required.

A sample-specific FE model was generated with the results obtained through image processing for both samples that were tested. A big difference between number of elements for a converged mesh of both samples can be noticed, which depends among others on the material parameters. This means that a mesh convergence study, using the material parameters obtained through classic parameter fitting, is required for every sample.

4.2 | Classic and BCC parameter fitting

In our previous study we proposed the BCC parameter fitting procedure and applied it to virtual data of a rake-based planar biaxial test[?]. We showed that the classic parameter fitting procedure was not capable of retrieving the ground truth material parameters, whereas the BCC parameter fitting procedure was. When applying the method to real experimental data, the ground truth material properties of the sample being tested are unknown and a full verification of the method is impossible. Though the virtual experiments contain simplifications with respect to real experiments, there is no reason to believe that these simplifications would affect the principle of the method.

From Figures 11 and 12 it can be observed that the result of the two cases of BCC parameter fitting is consistent: the correction for both samples is towards a more compliant stress-strain response than what is measured experimentally at the rakes. The two cases end up in different material parameters and a different response. However, the difference between the two cases is smaller than the difference with the classic parameter fitting result.
The convergence of the BCC parameter fitting can be assessed with RMSE_g, which reflects how much the correction vector of the current iteration changed with respect to the previous iteration. For both cases the RMSE_g decreases steadily, confirming a good convergence of the BCC method. During the last BCC iterations, the change in material parameters is small. Therefore, it might be that the stop criterion is too strict for these experiments. The MPE_C reflects the difference of the current material parameters with respect to the parameters obtained with the classic fitting procedure. The amount of difference is up to 19% and up to 12% for samples S1 and S2, respectively. In other words, the mistake of the classic parameter fitting result differs per experiment. This is in correspondence with the previous observations that the correction vector is dependent on the testing conditions, the loading protocol and the sample material being tested.

The $\text{RMSE}_{t,exp}$ reflects the difference between the experimental traction force from the biaxial test and from the FE simulation and can be used to assess the quality of the BCC parameter fitting results. Comparing these values between the different cases of the BCC method, the performance of BCC_i is better than BCC_b. Hence, using a sample-specific FE model leads to improved results than when using a simplified FE model. The $\text{RMSE}_{t,exp}$ is sensitive to the range of the forces that are present in the experiment and in the FE simulation. It can be observed that the last BCC iteration does not always correspond the lowest value of $\text{RMSE}_{t,exp}$. This is not necessarily a problem since the convergence of the method and the final solution can be considered as two separate things. It makes most sense to choose the final material parameters as those with the smallest $\text{RMSE}_{t,exp}$ value.

4.3 | General discussion

Some aspects of these planar biaxial experiments could be improved in the future. For example, different methods should be explored to measure the thickness without applying a pressure to the sample. Also the testing temperature should be raised to 37° to better emulate *in vivo* condition. Moreover, the preload was only applied at the beginning of each set, while a better protocol would be to apply the preload before every stretch cycle to avoid baseline drifts. Multiple cycles (also referred to as 'preconditioning') are applied to account for the softening effect of soft biological tissues. The last cycle shows a repetitive behavior and is usually used for further analysis and parameter fitting. In this case, however, we chose to select the first stretch cycle as this starts from a realistic unloaded reference state, as the reference state of the last cycle was not realistic. While these aspects are important and should be considered when performing experiments, the focus of the current paper lies on a new method to perform parameter fitting on experimental data, and not on the experimental data itself. Hence, the aforementioned aspects do not influence the main message of this work, namely the improved estimation of the sample's material behavior when using the BCC approach.

The GOH material model, designed to model arterial tissue, was chosen to model the two human aorta samples. The aorta is modeled as one homogeneous layer. In reality aortic tissue is composed out of three layers: the intima, the media and the

adventitia. Also, different material models have been developed for arterial tissue that are more biofidelic (e.g. using a stochastic fiber distribution). The BCC method and the methods presented in this paper are independent from the material model that is considered, and can thus be used with different material models. The only prerequisite is that the material model is implemented in a FE software (possibly via a user material subroutine).

An artery also contains residual stresses. The stress state at the beginning of a mechanical test is therefore not completely stress-free, though this is often neglected. Maes *et al.*[?] proposed a method to estimate material parameters from a planar biaxial test, while taking into account the residual stresses, using the constrained mixture approach as described by Bellini *et al.*[?].

Another limitation is the fact that damage that can occur for example at the rake holes, is not modeled. This would require extra damage material parameters to be calibrated. In a classic parameter fitting, damage at the rake holes is accounted for when markers are used to measure the deformation of the tissue. In the BCC parameter fitting this is not enough. In this case, the selected sets used for parameter fitting were chosen such that no visible damage was present in the sample.

A preload is applied at the beginning of each set to avoid sagging of the sample. When the preload is reached, this is considered the reference or undeformed state. Therefore, the experimental force-stretch curve does not pass through (0,0): at zero stretch there is a preload. Analytically, this preload cannot be taken into account easily, since the material has a non-linear stress-strain behavior. However, using an iterative method, the deformation that corresponds to this preload can be calculated using FE. This could be plugged in in the current method and can be a subject of future research.

Besides the Classic and BCC methods described here, inverse FE parameter fitting is also a method to calibrate material parameters. The image processing and the generation of the FE model developed in this study, can be used directly for inverse FE parameter fitting. The difference between BCC and inverse FE parameter fitting, lies in the calculation of the model component in the objective function. In BCC parameter fitting, t_{mod} is calculated analytically, while for inverse FE parameter fitting the model component is obtained via a FE simulation. This means is that if the objective function is evaluated x times, x simulations are required in inverse FE parameter fitting. BCC parameter fitting only requires y FE simulations, with y the number of BCC iterations until convergence is reached. As y is much smaller than x, the computational cost of the inverse FE parameter fitting outweighs the cost of the BCC parameter fitting method.

5 | CONCLUSION

This paper presents the first application to experimental data of the BCC parameter fitting procedure for a planar biaxial test using rakes. BCC is an abbreviation of Boundary Conditions Corrected and hence this method takes into account the boundary conditions of the planar biaxial test and the inhomogeneities they cause in the stress-strain field. The BCC method was previously proposed and proven to be effective for virtual experimental data[?]. For the application to real experimental data an automated image processing technique was developed to extract the sample contour, the insertion points of the rakes and their orientations, and the markers from an experimental picture using the contrast in the image. This information was then used to generate a sample-specific FE model of the experiment. Also a simplified FE model (for which no image processing is required) was constructed. The FE models were used in the BCC parameter fitting method to calculate a correction vector that compensates for the boundary conditions of the experiment.

Two cases of the BCC parameter fitting were investigated:

- BBC_b: basic BCC using a basic FE model
- BCC_i: image-based BCC using an image-based FE model

From these two variations to the BCC procedure it can be concluded that the correction of both cases is consistent: the actual stress at the center of the sample is in reality lower than the stress calculated from the forces measured at the rakes. Both cases end up in a different material parameter set and a different stress-strain response. The performance of the BCC method is assessed comparing the traction forces measured experimentally to those obtained from the FE model. BCC_i leads to a better approximation of the traction forces measured in the experiment. A scaling factor is required to calibrate the dimensions in the

experimental images. Apart from this scaling factor, no other information than the what is obtained in an normal planar biaxial test is required. Therefore, the method can be implemented easily and applied widely. The first application to experimental data shows that even the basic BCC approach leads to an improved estimation of the sample behavior.

6 | ACKNOWLEDGEMENTS

The authors would like to thank Maxim Van den Abbeele and Marija Smoljkić for using the data of their experiments. This work was supported by a post-doctoral fellowship of the Research foundation Flanders (FWO) (PDO-012) and a C2 project of internal KU Leuven funding (C24/16/026).

7 | BIBLIOGRAPHY